ENHANCED RADIATIVE DIVERTOR POWER EXHAUST THROUGH INJECTION OF LOW-Z POWDERS IN DIII-D

F. EFFENBERG, A. BORTOLON, R. LUNSFORD, A. NAGY, B.A. GRIERSON, F. LAGGNER, R. MAINGI, R. NAZIKIAN
Princeton Plasma Physics Laboratory
Princeton, New Jersey, USA
Email: feffenbe@pppl.gov

L. CASALI, I. BYKOV, H.Q. WANG, D.M. THOMAS
General Atomics
San Diego, California, USA

F. SCOTTI, M.E. FENSTERMACHER
Lawrence Livermore National Laboratory
Livermore, California, USA

H.G. FRERICHS
University of Wisconsin - Madison
Madison, Wisconsin, USA

J.D. LORE
Oak Ridge National Laboratory
Oak Ridge, Tennessee, USA

Y. FENG
Max-Planck-Institut für Plasmaphysik
Greifswald, Mecklenburg-Vorpommern, Germany

Abstract

Injection of non-recycling low to mid Z impurity powders has recently been introduced as a new technique to mitigate divertor heat fluxes and improve wall-conditioning at DIII-D, which are both of critical importance for the success of next-step fusion devices. This new technique enables extending the limited number of impurity species and mixtures usable with conventional gas injection. In this paper, the first radiative power exhaust experiments with impurity powder injection at the DIII-D tokamak are presented and discussed. Lithium (Li) and boron (B) powders were dropped with rates of 1-50 mg/s directly into the outer strike point located in the closed small angle slot (SAS) divertor during ELMy H-mode scenarios in upper single null, forward B_t configuration (I_p~1 MA, B_t=2 T, P_{NB} ~ 6 MW, f_{ELM} ~ 80 Hz, n_e ~ 3.6-5.0x10^{19} m^{-3}). The injection caused a substantial reduction in divertor electron temperature, particle fluxes, and heat fluxes, measured by Langmuir probes in the SAS. The strong increase of near-target neutral pressure supports transition into divertor detachment accompanied by an 8-10% degradation in H-mode energy confinement. The radiative power in the divertor scrape-off layer (SOL) was increased by 37% and 20% for Li and B, respectively. Measurements of the impurity line emission distribution with tangential cameras show the Li II radiation concentrated along the separatrix leg in the divertor region. In contrast, the B II emission is concentrated in remote parts of the SOL and attached to the divertor plates. EMC3-EIRENE modeling of the radiative power exhaust with lithium and boron based on atomic data from ADAS recovers features of the experimental emission distributions. The analysis shows that the ionization and species-dependent cooling potentials explain the distribution of power losses, which may cause differences in the details of the divertor plasma distribution measured with Langmuir probes. Li is found to radiate close to the hot separatrix, while B radiative losses occur more rooted in the SOL and close to the divertor. The results show that low Z powder injection is a novel and effective method that enhances divertor dissipation and promotes detachment while maintaining good energy confinement in high-performance discharges.

1. INTRODUCTION

Present plasma-facing component (PFCs) materials cannot withstand heat fluxes above 10 MW/m^2 predicted for the next step large-scale fusion reactors such as ITER [1] or a projected future US fusion pilot power plant [2]. Dissipation and spreading of heat fluxes by isotropic low Z impurity line emission is a promising technique to

prevent melting and damage and extend the lifetime of the exposed wall materials. Currently, tungsten is the high Z material choice for the ITER divertor and recent and future world-leading reactor experiments [3], [4]. Low to mid Z impurities have to be injected in a controlled manner to enhance the radiation in the boundary of fusion plasmas and reduce the heat and particle fluxes to the target plates [5]. The ideal regime would be a high-performance core, a stable H-mode upstream, and a cold and dense divertor downstream. The radiative power losses by low Z impurities reduce the temperature down to values that enable volume recombination and the creation of a protective neutral gas cushion in front of the targets. In such a regime, the plasma is detached from the divertor targets, and heat and particle loads suppressed [6]. The conventional approach widely investigated at tokamaks and stellarators is to inject impurities in gaseous form to reduce heat fluxes and achieve detachment in a controlled way. The choice of gases is determined by their radiation characteristics and may be limited by nuclear chemistry [7], [8]. The leading candidates are nitrogen and neon since their temperature-dependent peak radiation is concentrated in the scrape-off layer (SOL) and around the separatrix, respectively. However, numerical studies have shown that alternative impurities such as boron (B) may deserve consideration as well [9]. Yet, toxicity limits the application of B in gas form. Lithium (Li) is another candidate of interest that is also predicted to be effective for heat flux dissipation in a lithium vapor box divertor design [10]. An alternate approach is to replace solid material walls with a flowing liquid lithium wall which potentially allows to spread and conduct heat efficiently and safely away [11]. Both Li and B are also used for wall-conditioning to reduce oxygen content and lower recycling for density control and performance increase. Traditionally, walls were lithiumized and boronized by evaporation and the glow discharge technique, respectively. More recently, the impurity powder injection technique was introduced as a novel technique to allow for the injection of alternative impurities in solid form for various real-time applications. First applications focused on real-time wall conditioning and the mitigation of edge localized modes (ELMs) which have been demonstrated with B, BN, and Li powders at DIII-D, EAST, ASDEX-U, and KSTAR [12]–[15].

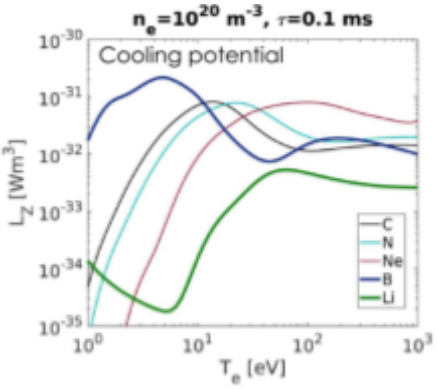

FIG. 1. Cooling potential for carbon, nitrogen, neon, boron, and lithium.

In the present paper, first-time experiments at the DIII-D tokamak are presented where radiative power enhancement was achieved during H-mode by injecting lithium and boron impurity powders into the upper closed small angle slot divertor. A set of edge diagnostics was used to provide a first assessment and analysis of two representative shots with Li and B, respectively. A description of the experimental setup, the method, the experimental scenario, and the first interpretation by modeling will be provided in the following.

2. RADIATIVE DISSIPATION WITH LOW TO MID Z IMPURITY INJECTION

Impurity seeded divertor power exhaust, and radiative mantle experiments generally rely on low to mid Z impurities due to their capability to radiate at edge temperatures up to a few hundred electron volts avoiding substantial energy losses in the confinement region. The temperature dependence of the respective cooling capabilities is represented by the cooling potential shown in figure 1. Here, the curves of carbon, nitrogen, neon, lithium, and boron are compared against each other. The emission has been calculated with atomic data from ADAS [16]. Carbon is an intrinsic impurity in DIII-D typically released from graphite PFCs into the plasma edge by chemical or physical erosion processes. It is very suitable for plasma edge cooling since its radiation zone extends over several tens of eV. However, graphite is not a material option for nuclear environments due to tritium retention associated with the co-deposition of hydrocarbons. The current choice of tungsten as a leading material candidate requires consideration of alternative edge radiators. Nitrogen is the closest to carbon in terms of radiation characteristics. However, nitrogen should be kept to a minimum due to the production of tritiated ammonia, which contaminates the uranium beds of the tritium plant. Neon is of interest because it is a non-reactive high-recycling noble gas well suited for radiative mantle power exhaust. Radiative power exhaust with the aforementioned conventional radiators have been extensively investigated at TEXTOR, JET, ASDEX, DIII-D, LHD, and more recently at Wendelstein 7-X [5], [17]–[21].

The introduction of real-time powder injection extends the range of impurity species for radiative power exhaust. Impurities in powder form facilitate pure boron application in contrast to gas delivery that requires toxic or explosive gases like diborane (B_2D_6) or strongly diluted compounds such as trimethyl borane (C_3D_9B). It also facilitates the use of lithium as well as multi-species mixtures such as boron nitride. It generally delivers impurities in higher purity without the bonding to fuel and other unwanted impurities, as in the case of molecular gases.
The cooling potential of boron and lithium in figure 1 shows the opposite evolutions. Boron mostly radiates at temperatures below 10 eV, while lithium shows maximum radiation above 50 eV, similar to neon (yet has another peak below 1 eV). In addition to their power exhaust capabilities, boron and lithium are also used for wall conditioning.

3. THE CLOSED DIVERTOR H-MODE SCENARIO

The experiments discussed in the following were conducted in upper-single null ELMy H-mode in forward B_t direction (Ip~1 MA, B_t=2 T, P_{NB}~6 MW, f_{ELM}~80 Hz, n_e~3.6-5.0x1019 m-3). The outer strike point (OSP) is positioned in the small-angle slot divertor and the ion grad-B drift direction points away from the SAS. in this configuration. Figure 2 shows the magnetic equilibrium, the location of the OSP at the SAS target, the injection location (green arrow), and the divertor diagnostics. The box in figure 2 shows the SAS geometry in more detail, including the array of Langmuir probes (LP), the position of Pressure Gauge (PG), and the injection tube of the impurity powder dropper (IPD) [22], [23].
The versatile impurity powder dropper (IPD) [24] is mounted at the top of the DIII-D tokamak device at a toroidal angle of 195°. It has four reservoirs filled with different types of impurity powders and granules. Impurity powders were dropped directly into the OSP region through a tube into the SAS. The divertor Langmuir probes and pressure gauge are used to characterize the divertor plasma. Besides, tangential camera diagnostics equipped with narrow bandpass interference filters measure line integrated brightness of different charge states of injected impurities [25]. The closed divertor geometry generally facilitates the dissipation of heat and particle fluxes due to inherently better neutral compression [22], [23], [26].

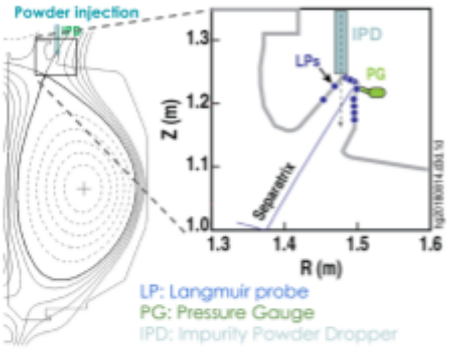

FIG. 2. The outer strike point is located in the small-angle slot divertor (SAS) in this Upper Single Null (USN) H-mode equilibrium. The impurity powder dropper is connected to the SAS divertor by a tube (cyan). The box shows the locations of the Langmuir probe (LP) array, the pressure gauge (PG) and the impurity powder dropper (IPD) in the SAS.

4. DIVERTOR POWER EXHAUST WITH LITHIUM AND BORON POWDERS

4.1 Substantial increase in divertor neutral pressure while maintaining H-mode

In a sequence of experiments, lithium and boron were injected for the first time for the purpose of radiative power exhaust in H-mode (see FIG. 3). The impurity powder is injected gravitationally at 2.2 s. It falls with a velocity of ~5 m/s through a ~2 m long tube and reaches the plasma at ~3.2 s. The powder size varies in a range of 2-100 μm. Mass flow rates of 1-50 mg/s were determined with a flowmeter. Two representative shots #176750 and #176744, with Li and B injection, are discussed in the following. Accurate matching of flow rates was not possible at this point since some shots showed additional MHD activity perturbing the analysis. These two shots discussed show comparable conditions and are best cases for comparison. The injection rates were 3.3 mg/s and 35 mg/s for Li and B, respectively (~ 10^{20} - 10^{21} at./s). The traces of main discharge parameters are shown in figure 3 for density, injected neutral beam power, energy confinement time, effective charge, radiative power near divertor, and divertor neutral gas pressure.

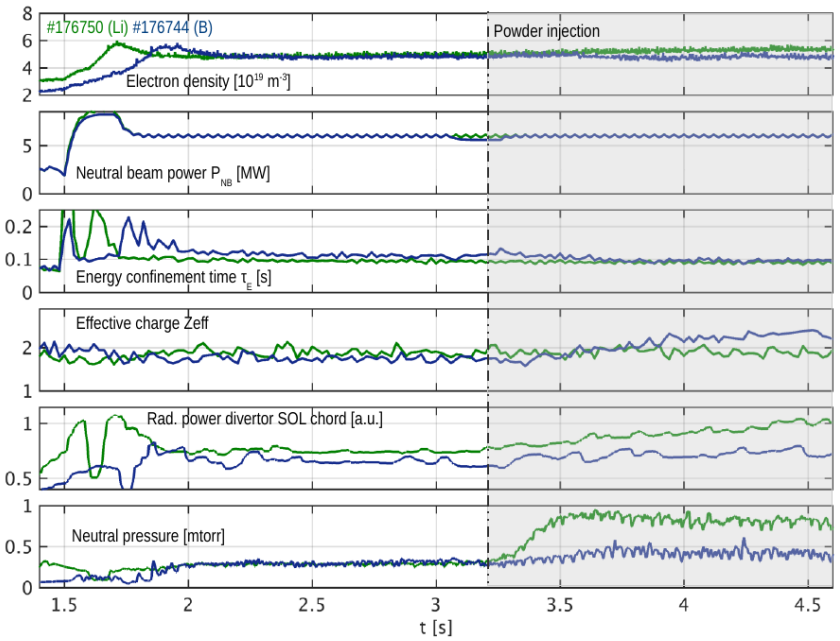

FIG. 3. Time traces of representative discharges with lithium and boron injection showing line averaged density n_e, neutral beam power P_{NB}, energy confinement time τ_E, effective charge Z_{eff}, divertor SOL radiation, and divertor neutral pressure.

The overview shows that upstream plasma parameters remain almost unchanged during the injection. In contrast, the divertor pressure shows a substantial increase by nearly a factor of three in the case of lithium and by a factor of 1.5 in the case of boron. Such an increase in divertor pressure has been associated with increased dissipation and transition to detachment earlier [23]. A marginal increase in the line averaged density by 5% is measured in the case of Li, while it drops by ~8% in the case of B injection. Only marginal losses in energy confinement of -8% and -10% are observed for Li and B, respectively. Boron injection results in an increase of the effective charge by 50% indicating core dilution. The radiation in the vicinity of the SAS enhances by 37% and 20% for Li and B, respectively. The base-level divertor SOL radiation prior to powder injection is roughly a factor of two higher than the core one. The results show that low Z powders are suitable to enhance divertor neutral pressure during high confinement mode without perturbing the core performance significantly. Thereby, impurity powders offer similar capability as low Z impurity gases as reported in [18].

3.2 Differences in spatial distributions of lithium and boron emission

Components of the spatial lithium and boron emission distributions are captured during powder injections with the tangential camera. The filters applied extract Li II at 546 nm and B II at 410 nm. Since D-delta and C III emit within the bandpass of the filter used to image boron emission, background emission before boron injection was subtracted from the camera images. Some residual contaminating emissivity might remain due to emissivity changes resulting from local cooling from the injected powder. The spatial brightness distributions are shown in figure 4. The top views show the raw camera data, and the bottom images show the projection, including the in-vessel geometry to provide a better orientation regarding the SAS geometry. The Li II radiation is concentrated along the outer divertor leg. The high-intensity region extends from the SAS volume to the X-point. This means that the Li radiation zone is located in the hotter parts around the separatrix. The B II emission shows a different distribution. It peaks

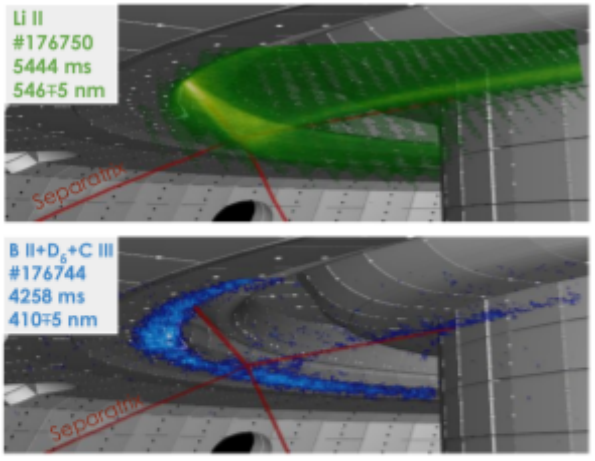

FIG. 4. Tangential camera view on Li II at 546 nm (left) and B II at 410 nm (right) during the injections. The boron filter also captures D_δ and C III emissions. Background subtraction was undertaken, but some residual emissivities from hydrogen and carbon might remain since the cooling effects may change the intensities.

close to the PFCs and extends in a radial direction outwards near the targets. The distinct features of the emission distribution of Li and B appear to reflect the temperature dependency of the cooling potentials shown in figure 1. Analysis by modeling in the following will show that the distributions of Li II and B II are representative for the impurity species-dependent power losses in different domains of the SOL. Boron cools the SOL while lithium causes temperature reduction in the vicinity of the separatrix.

4.3 Drop of divertor temperature and divertor detachment

The divertor plasma has been characterized with a Langmuir probe array embedded in the SAS targets (compare figure 2). The evolution of divertor electron temperature Te, electron density n_e, perpendicular heat flux $q_\perp$, and particle flux (expressed as ion saturation current) J_{sat} are shown in figure 5 for Li and B powder injection, respectively. A sudden transition occurs after ~3.2 s when the powder reaches the divertor plasmas. Example profiles for the respective plasma are shown in figure 5 (reight) before (2.9 s) and during powder injection (3.7 s). The Li injection case shows a rapid reduction in electron temperature followed by an increase in divertor density. The peak heat flux reduces by 50% while the ion saturation current is slightly enhanced. The results suggest that Li increases the density and cools the divertor without detaching the particle flux.

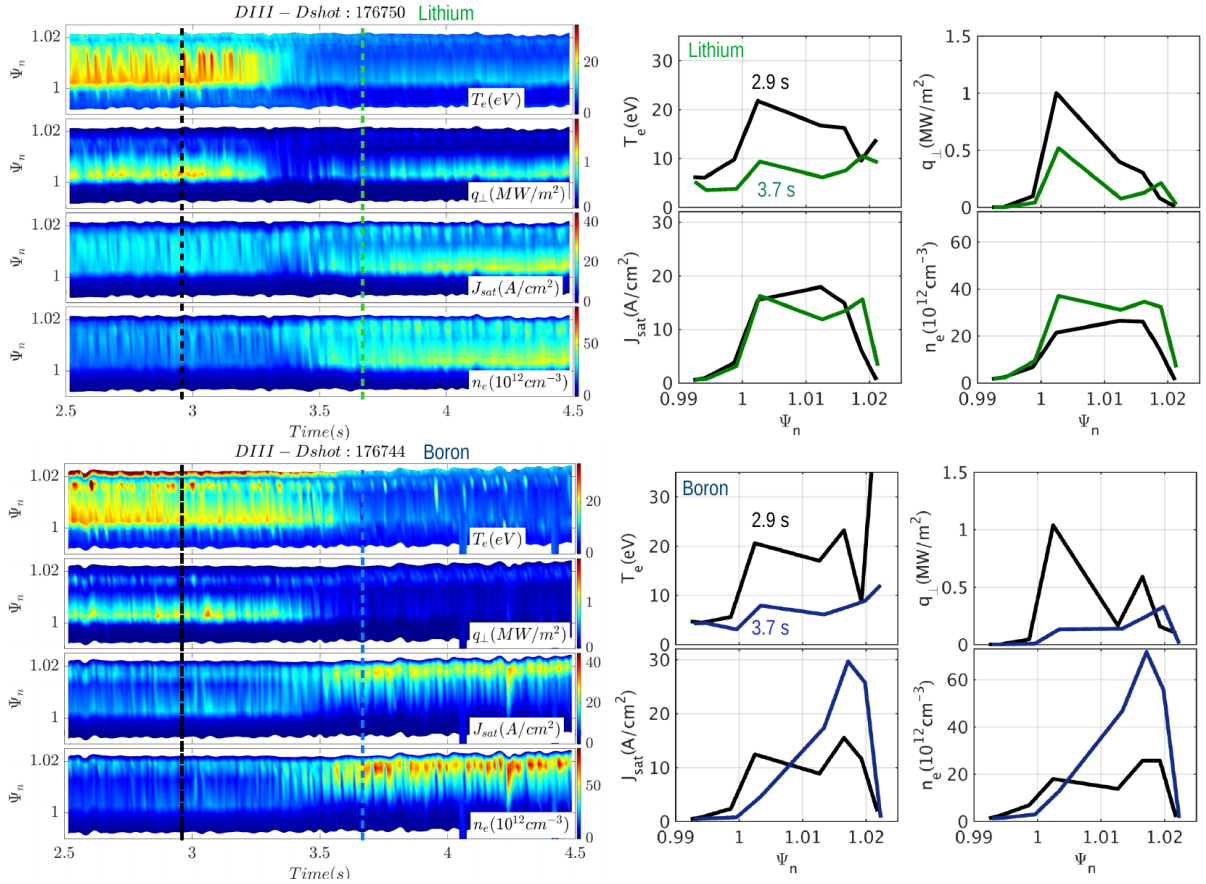

FIG. 5. Divertor Langmuir probe traces for electron temperature T_e, perpendicular heat flux $q_\perp$, particle flux J_{sat}, and density for cases with lithium (top) and boron (bottom) injection. The powders enters the divertor plasma at 3.2 s (dashed green and blue lines). Example profiles are shown on the right before (2.9 s) and during powder injection (3.7 s).

B powder injection results in a slightly different response of divertor plasma parameters, as shown in figure 5 (bottom panels). Te drops to ~5 eV and $q_\perp$ nearly vanishes at the strike point after 3.2 s while n_e and Jsat increase in the far SOL (ψ_n>1.01). This suggests that boron is effective to reduce both the temperature and heat flux while it causes a denser plasma in the far SOL.

Both lithium and boron significantly reduce the divertor electron temperature and detach the heat flux. The differences most obvious in the resulting divertor density and particle flux distributions may be a species-dependent effect. Dissipation is supposed to occur in different parts of the SOL according to the cooling

potentials shown in figure 1. This may affect the local pressure balance and eventually the particle fluxes to the targets. The species dependence of total radiative losses will be discussed in the following based on edge impurity transport modeling.

5. FIRST EDGE MODELING OF LITHIUM AND BORON ASSISTED RADIATIVE POWER EXHAUST

To study the radiation characteristics, radiation efficiency, and spatial distribution of the Li and B impurities, these scenarios have been analyzed with the 3D plasma-fluid and kinetic neutral edge transport code EMC3-EIRENE [27]. In the first step, a representative equilibrium has been implemented for shot #176750. Edge transport simulations have been conducted for different densities keeping the input power of 6 MW fixed. Two cases with a fixed separatrix density of $2 \cdot 10^{19}$ m^{-3} are examined in the following for Li and B. The impurity line emission was modeled using atomic data from ADAS [16]. The power loss fraction was fixed to 0.4 to have comparable dissipation and resolve the efficiency of the radiators. It has to be noted that drift effects are not yet implemented in EMC3-EIRENE. The 2D emissivity patterns for total Li and B power losses, Li II and B II, and their line integrated brightness obtained by synthetic camera diagnostic modeling [28] are shown in figure 6.

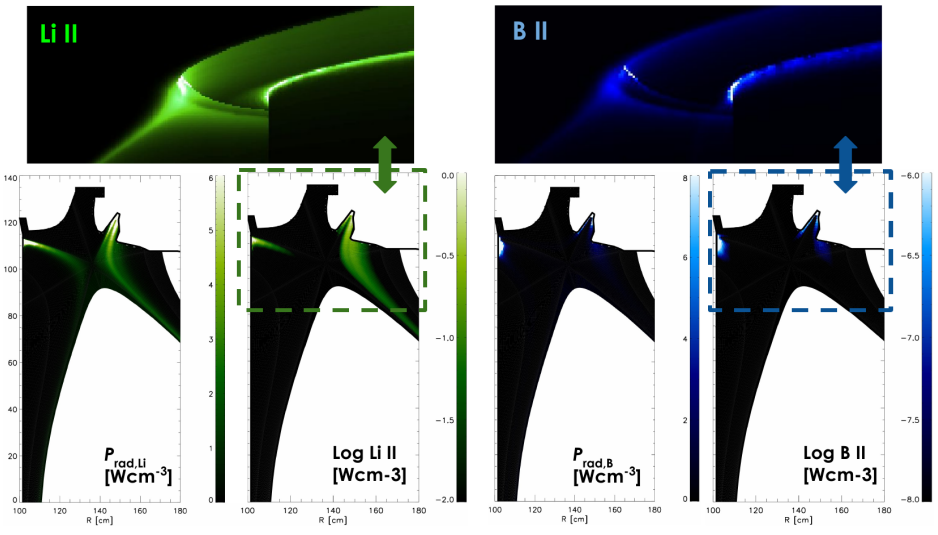

FIG. 6. Modeling of total radiated power P_{rad} for Li and B, and Li II and B II line emission distributions with EMC3-EIRENE. The 2D distributions show similar Li radiation being more extended along the divertor legs and separatrix while B emission peaks close to the targets. A synthetic camera (top) shows the line integrated brightness according to the experimental tangential camera view. Differences between experiment and modeling result from the more even distribution of the modeled impurity sources.

The Li radiation is concentrated near the separatrix and at the strike line, while the B peak emission front is concentrated in the far SOL and in the recycling region. These characteristic features, qualitatively consistent with spectral divertor imaging measurements, result from the different cooling efficiencies of these two impurities combined with transport effects. The modeling shows relatively flat target electron temperature profiles in the case of low-Z impurity radiation (f_{rad}=40%). The differences between experimentally measured line emission (compare figure 4) and modeling are due to the simplifying assumption of axisymmetric impurity sourcing from the tor 1argets in the main recycling regions. The ideal assumptions in the modeling are based on atomic data from ADAS (as in the case of the cooling potentials shown in figure 1) and recover characteristic features observed in the experiment. The modeling results show that B+1, B+2, Li+1, and Li+2 are the main edge dissipators. Therefore, the distribution of Li II and B II emission indicates the spatial distribution of the power losses in the plasma boundary. Both Li and B are found to reduce the target electron temperatures and heat fluxes in the closed divertor substantially. The modeling reveals that B is a more efficient radiator concerning the power losses induced by a specific injection rate. E.g., the total radiated power per impurity influx by Li is ~35 W/A and ~880 W/A for B. The modeled impurity line emission shows very similar effects as observed experimentally and supports the interpretation that major differences in the line emission distribution are linked to the species-dependent cooling potentials. Boron, in particular, may give access to a dissipative divertor plasma regime with power losses rooted more profound in the SOL. The promising trend suggests that

complete modeling of non-symmetric local impurity sources will recover plasma and impurity distribution better matching with experimental observations.

6. SUMMARY AND CONCLUSIONS

Radiative power exhaust with lithium and boron powders has been demonstrated for the first time at DIII-D. The experiments have been conducted in a USN closed divertor (SAS) configuration during 6 MW ELMy H-mode. The measurements showed only a marginal decrease in energy confinement time while divertor radiation increased. Both lithium and boron caused substantial pressure increase by a factor of 3 and 1.5, respectively, while divertor temperatures and heat fluxes were reduced while divertor is detached transiently during powder injection.

Differences in the divertor plasma parameters, in particular density and ion saturation current profiles, are likely related to the differences in the distribution of radiative losses, which cool different parts of the SOL. This is reflected in lithium and boron cooling potentials and the Li II and B II emissivity distributions measured. Lithium radiates at higher temperatures around the separatrix while boron emission is rooted in the SOL and close to the targets. The principal radiation features observed in the experiment are also recovered in the first modeling with EMC3-EIRENE. Modeling shows a characteristic radiation distribution similar to the experiment despite the ideal axisymmetric assumption. The lower impurity charge states (Z=+1, +2) are the main contributors to radiative dissipation in the edge. A reduction and flattening of electron temperature are achieved at f_{rad}=40% with both Li and B. Boron is an order of magnitude more efficient radiator than lithium and allows for power losses rooted deep in the divertor SOL.

More sophisticated modeling is needed to recover any local source effects and the details of the heat and particle flux distribution in the small angle slot divertor. Further data analysis will focus on other impurity species and the effects on ELMs.

The presented results show that low Z powders are as effective as conventional low Z impurity gases for enhanced divertor dissipation and improved core-edge compatibility.

ACKNOWLEDGEMENTS

This material is based upon work supported by the U.S. Department of Energy, Office of Science, Office of Fusion Energy Sciences, using the DIII-D National Fusion Facility, a DOE Office of Science user facility, under Awards DE-AC02-09CH11466, DE-FC02-04ER54698, DE-AC52-07NA27344, DE-FG02-07ER54917, DE-SC0020357 and DE-AC05-00OR22725.

REFERENCES

[1] R. A. Pitts et al., “A full tungsten divertor for ITER: Physics issues and design status,” J. Nucl. Mater., vol. 438, pp. S48–S56, 2013, doi: https://doi.org/10.1016/j.jnucmat.2013.01.008.
[2] National Academy of Engineering and E. National Academies of Sciences and Medicine, Bringing Fusion to the U.S. Grid. Washington, DC: The National Academies Press, 2021.
[3] C. Linsmeier et al., “Development of advanced high heat flux and plasma-facing materials,” Nucl. Fusion, vol. 57, no. 9, p. 092007, 2017, [Online]. Available: http://stacks.iop.org/0029-5515/57/i=9/a=092007.
[4] J. W. Coenen et al., “Materials for DEMO and reactor applications—boundary conditions and new concepts,” Phys. Scr., vol. 2016, no. T167, p. 014002, 2016, [Online]. Available:

http://stacks.iop.org/1402-4896/2016/i=T167/a=014002.
[5] G. P. Maddison et al., “Moderation of divertor heat loads by fuelling and impurity seeding in well-confined ELMy H-mode plasmas on JET,” Nucl. Fusion, vol. 51, no. 4, p. 042001, 2011, [Online]. Available: http://stacks.iop.org/0029-5515/51/i=4/a=042001.
[6] G. F. Matthews, “Plasma detachment from divertor targets and limiters,” J. Nucl. Mater., vol. 220–222, pp. 104–116, 1995, doi: https://doi.org/10.1016/0022-3115(94)00450-1.
[7] A. Kallenbach et al., “Impurity seeding for tokamak power exhaust: from present devices via ITER to DEMO,” Plasma Phys. Control. Fusion, vol. 55, no. 12, p. 124041, Nov. 2013, doi: 10.1088/0741-3335/55/12/124041.
[8] R. J. Walker and M. R. Gilbert, “Neutron activation of impurity seeding gases within a DEMO environment,” Fusion Eng. Des., vol. 124, pp. 892–895, 2017, doi: https://doi.org/10.1016/j.fusengdes.2017.01.057.
[9] A. Yu. Pigarov, “Radiative detached divertor with acceptable separatrix Z eff,” Phys. Plasmas, vol. 24, no. 10, p. 102521, Oct. 2017, doi: 10.1063/1.4986516.
[10] R. J. Goldston, R. Myers, and J. Schwartz, “The lithium vapor box divertor,” Phys. Scr., vol. T167, p. 014017, Feb. 2016, doi: 10.1088/0031-8949/T167/1/014017.
[11] D. N. Ruzic et al., “Flowing liquid lithium plasma-facing components – Physics, technology and system analysis of the LiMIT system,” Nucl. Mater. Energy, vol. 12, pp. 1324–1329, Aug. 2017, doi: 10.1016/j.nme.2017.06.001.
[12] A. Bortolon et al., “Observations of wall conditioning by means of boron powder injection in DIII D H-mode plasmas,” Nucl. Fusion Accept., 2020, [Online]. Available: http://iopscience.iop.org/10.1088/1741-4326/abaf31.
[13] R. Maingi et al., “ELM elimination with Li powder injection in EAST discharges using the tungsten upper divertor,” Nucl. Fusion, vol. 58, no. 2, p. 024003, Jan. 2018, doi: 10.1088/1741-4326/aa9e3f.
[14] A. Bortolon et al., “Real-time wall conditioning by controlled injection of boron and boron nitride powder in full tungsten wall ASDEX Upgrade,” Nucl. Mater. Energy, vol. 19, pp. 384–389, 2019, doi: https://doi.org/10.1016/j.nme.2019.03.022.
[15] E. Gilson and et al., “Wall Conditioning and ELM Mitigation with Boron Nitride Powder Injection in KSTAR,” Journal of Nuclear Materials and Energy, submitted 2021.
[16] H. P. Summers et al., “Atomic data for modelling fusion and astrophysical plasmas,” Plasma Phys. Control. Fusion, vol. 44, no. 12B, p. B323, 2002, [Online]. Available: http://stacks.iop.org/0741-3335/44/i=12B/a=323.
[17] U. Samm et al., “Radiative edges under control by impurity fluxes,” Plasma Phys. Control. Fusion, vol. 35, no. SB, pp. B167–B175, Dec. 1993, doi: 10.1088/0741-3335/35/sb/013.
[18] L. Casali et al., “Improved core-edge compatibility using impurity seeding in the small angle slot (SAS) divertor at DIII-D,” Phys. Plasmas, vol. 27, no. 6, p. 062506, Jun. 2020, doi: 10.1063/1.5144693.
[19] T. Morisaki et al., “Radiated power distributions in impurity-seeded plasmas in LHD,” J. Nucl. Mater., vol. 463, pp. 640–643, 2015, doi: http://dx.doi.org/10.1016/j.jnucmat.2015.01.016.
[20] F. Effenberg et al., “First demonstration of radiative power exhaust with impurity seeding in the island divertor at Wendelstein 7-X,” Nucl. Fusion, vol. 59, no. 10, p. 106020, Aug. 2019, https://doi.org/10.1088/1741-4326/ab32c4.
[21] A. Kallenbach et al., “Partial detachment of high power discharges in ASDEX Upgrade,” Nucl. Fusion, vol. 55, no. 5, p. 053026, May 2015, doi: 10.1088/0029-5515/55/5/053026.
[22] H. Y. Guo et al., “First experimental tests of a new small angle slot divertor on DIII-D,” Nucl. Fusion, vol. 59, no. 8, p. 086054, Aug. 2019, doi: 10.1088/1741-4326/ab26ee.
[23] M. W. Shafer et al., “Dependence of neutral pressure on detachment in the small angle slot divertor at DIII-D,” Nucl. Mater. Energy, vol. 19, pp. 487–492, May 2019, doi: 10.1016/j.nme.2019.04.003.
[24] A. Nagy et al., “A multi-species powder dropper for magnetic fusion applications,” Rev. Sci. Instrum., vol. 89, no. 10, p. 10K121, 2018, doi: 10.1063/1.5039345.
[25] M. E. Fenstermacher, W. H. Meyer, R. D. Wood, D. G. Nilson, R. Ellis, and N. H. Brooks, “A tangentially viewing visible TV system for the DIII-D divertor,” Rev. Sci. Instrum., vol. 68, no. 1, pp. 974–977, Jan. 1997, doi: 10.1063/1.1147729.
[26] L. Casali, D. Eldon, J. A. Boedo, T. Leonard, and B. Covele, “Neutral leakage, power dissipation and pedestal fueling in open vs closed divertors,” Nucl. Fusion, vol. 60, no. 7, p. 076011, Jul. 2020, doi: 10.1088/1741-4326/ab8d06.
[27] Y. Feng et al., “Recent Improvements in the EMC3-Eirene Code,” Contrib. Plasma Phys., vol. 54, no. 4–6, pp. 426–431, 2014, https://doi.org/10.1002/ctpp.201410092.
[28] H. Frerichs et al., “Synthetic plasma edge diagnostics for EMC3-EIRENE, highlighted for Wendelstein 7-X,” Rev. Sci. Instrum., vol. 87, no. 11, p. 11D441, 2016, https://doi.org/10.1063/1.4959910.